ELSEVIER

Contents lists available at ScienceDirect

Optical Fiber Technology

journal homepage: www.elsevier.com/locate/yofte



Regular Articles

Assessing client-side protection impact on C+L+S multi-band optical networks with a GNPy-based planning tool

Rodrigo Guerreiro a, Luís Cancela a,b, João Rebola a,b,

- ^a Iscte Instituto Universitário de Lisboa, Lisbon, Portugal
- b Optical Communications and Photonics Group, Instituto de Telecomunicações, Lisbon, Portugal

ARTICLE INFO

Keywords: GNPy tool Multi-band Optical networks Optical protection Routing, modulation format and spectrum assignment

ABSTRACT

Multi-band (MB) transmission is a solution capable of increasing optical networks capacity and surpassing C-band transmission limitations. However, as more capacity is transported in these new MB networks, survivability and energy consumption issues become more relevant. This work investigates the impact of those issues in C+L+S MB optical networks using a tool based on the Gaussian noise Simulation in Python (GNPy) tool. The routing, modulation format and spectrum assignment (RMSA) algorithm provided in the GNPy tool is improved to take into account both client-side dedicated protection and inter-channel stimulated Raman scattering-Gaussian noise model. The protection level impact on the network performance is assessed by performing several RMSA studies on the German network for different protection levels and two blocking probabilities. Our results indicate that increasing the protection level by 25% leads to an 11% decrease in transported capacity and a 4% increase in spare capacity, with a 1 dBJpTbit increase in energy consumption per Tbit. Also, it is shown that these capacities become approximately stabilized above a 75% protection level. Despite the transported capacity in the C+L+S-band significantly increases compared to the C+L-band scenario, the energy consumption per Tbit remains almost the same in both scenarios.

1. Introduction

With the arrival of new technologies and services such as cloud, 5G, and Internet of Things, which are bringing a large number of new devices into networks, and the increasing popularity of streaming services, the network traffic continues to experience a massive growth [1]. Therefore, there is a need to increase the capacity of optical fiber networks, the telecommunications infrastructure that supports the majority of the internet data traffic flow around the world.

To accomplish such data capacity demand, the spectral efficiency of the single mode fiber (SMF) using the C-Band (1530 nm to 1565 nm), the band that is currently being used in most commercial optical networks, is approaching the theoretical Shannon limit. Coherent detection that allows using quadrature amplitude modulation (QAM) formats, elastic optical networks, and flexible grid are no longer providing significant capacity enhancement in optical networks [2–4].

Currently, two solutions are being pursued to solve this data capacity crunch in optical networks. The first one uses space division multiplexing (SDM) in the optical domain [2,4], while the second one, which is called the multi-band (MB) solution, explores other bands in a SMF than the C-band [4].

In this work, we focus on the MB solution, which increases the network capacity by utilizing other bands beyond the C-band, specifically the O-, E-, S-, and L-bands, that have an attenuation coefficient below 0.4 dB/km [3]. Some commercial transmission systems are already using optical links that use the C+L-band, like Infinera's *FlexILS* solution [5] and Google is deploying the C+L MB solution globally in their long-haul terrestrial networks [6]. More recently, in 2024, a record transmission using a MB system in standard commercially available optical fiber was reported, reaching a record data-rate of 402 Tbit/s after 50 km, using a bandwidth of 37.6 THz, covering the O-E-S-C-L-U-bands [7]. Using more bands can increase the network bandwidth up to its limit, approximately 50 THz, more than ten times the C-band bandwidth [8].

MB networks, besides increasing data capacity, bring new challenges to the network physical layer, at the transmission level, by enhancing the effect of inter-channel stimulated Raman scattering (ISRS), which is negligible in the C-band [3,9,10], or by using devices whose features are band-dependent [2]. Furthermore, at the device level, with higher capacities and more bands, the network nodes become more complex and must have larger dimensions [2]. The overall immaturity of MB components is also a critical aspect in the design and cost

E-mail addresses: rfgoo@iscte-iul.pt (R. Guerreiro), luis.cancela@iscte.pt (L. Cancela).

^{*} Corresponding author.

of a MB network [2–4,11]. Regarding the network layer, the MB networks require new planning tools to solve the routing, modulation format and spectrum assignment (RMSA) problem, which must address the particular features of the MB physical layer and the new bands available.

Besides the challenges referred in the previous paragraph, as MB networks allow a much higher transport capacity than C-band networks [8], it is imperative to consider, adapt, and improve optical protection techniques, not only in the network lifetime, but also in the planning phase. The impact of protection on the design and planning of C-band optical networks has already been extensively analyzed in the literature, e.g. [12,13]. Moreover, several authors have already started addressing the impact of optical protection on MB optical networks, e.g. [14-17]. In [14], a client-side protection scheme is considered in a C+L scenario with SDM, and both heuristics and Integer Linear Programming tools are used to study the impact of protection on the optical network metrics. In [15], the authors studied the network performance for different levels of partial migration from the C-band to the C+L-band scenario, using two protection schemes, dynamic restoration and dedicated protection. In [16], the focus is again on the survivability of networks with partial migration from the C to C+L scenario, but an adapted protection technique to operate the network more efficiently is proposed. More recently, in [17], the C+L+S scenario was studied considering several protection schemes and a new protection scheme that uses different adaptive path provisioning schemes has been proposed, considering an optical node with wavelength conversion to enable switching between bands. However, the use of wavelength converters inside an optical node is still an immature option for short-term deployment in the field [11].

Besides optical protection, energy consumption is also an important challenge in MB networks. It is well known that the Information and Communication Technology sector has a substantial contribution to the increase of worldwide ${\rm CO}_2$ emissions and MB technology, as it uses more bands and more devices, leads to a higher energy consumption [18]. So, it is crucial to assess the impact of network energy consumption in MB optical networks.

Despite the valid contributions from the previous works [14–17], that consider the impact of some protection schemes on MB scenarios and present a comparison performance study between the no protection and the full protection scenarios, to the author's best knowledge, the impact of client-side protection level on the planning of MB networks, and its relation with the network energy consumption has not yet been addressed and quantified in the literature.

In this paper, a planning tool, based on the Gaussian noise Simulation in Python (GNPy) tool [19], is adapted to consider network protection and used to address the RMSA problem in C+L+S MB networks considering different levels of client-side dedicated protection. The ISRS-Gaussian noise (GN) model is also implemented in the tool for optical signal-to-noise ratio (OSNR) estimation. The simulation results obtained for the German network are analyzed and conclusions on how the protection level impacts the network metrics, such as transported capacity, spare capacity, blocking probability (BP), and energy consumption per Tbit are drawn. A comparison performance is made with the C+L MB network scenario. The effects of different traffic patterns on the network metrics are also analyzed for the full protection scenario.

This paper is organized as follows. Section 2 provides a brief review on the main protection schemes in optical networks, highlighting the client-side scheme pros and cons. In Section 3, the GNPy-based planning tool for survivable C+L+S MB networks is presented, with a focus on the improvements made to accommodate the ISRS-GN model and the different protection levels. In Section 4, the simulation parameters and the RMSA simulator validation for an unprotected scenario are presented. Section 5 shows the simulation results for the German network, regarding the transported and spare capacities, as well as the energy consumption, considering the C+L+S band scenario and several levels of optical protection. It also presents the impact of the traffic pattern on a fully protected C+L+S network. Lastly, Section 6 presents the main conclusions of this work.

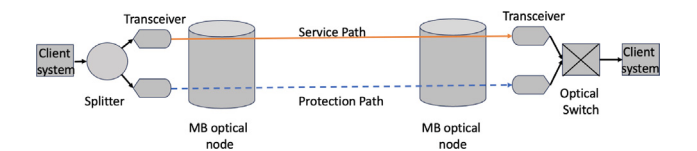


Fig. 1. Client-side 1+1 dedicated protection scheme.

2. Optical protection schemes

Optical networks must be robust against failures, whether due to cuts in connections or equipment malfunctions, as they transport vast amounts of data. Implementing protection mechanisms against these events enhances the availability of the network [20].

There are two well-known protection techniques, path protection and link protection [20]. Path protection is the most used, where a disjoint protection path from the source to the destination is used [20]. Path protection can be either dedicated or shared. Dedicated protection can be implemented as 1+1 or 1:1 [20]. In the 1+1 protection scheme, there are two live connections and, despite being more costly than 1:1 scheme gives an almost immediate response to a failure in the service path. The 1:1 protection scheme only sends the signal through the protection path in case of failure, which is more time consuming than the 1+1 protection scheme.

The protection mechanisms just referred can be implemented at the client-side or at the network-side. Concerning 1+1 dedicated protection, client-side protection requires two pairs of transceivers, as shown in Fig. 1, but can achieve the highest network survivability, and potentially allows reducing the spectrum used since different modulation formats can be used for both the service and protection paths [12,13]. On the other hand, network-side protection needs only one pair of transceivers and solves the failures more quickly [14], but the same signal must be used on both service and protection paths, since the most stringent path, usually the protection path, constrains the modulation format used. In this work, we use client-side 1+1 dedicated protection, as it has a higher survivability than network-side schemes, allows reducing the used spectrum, and has a faster response than the 1:1 protection scheme [20].

3. GNPy-based planning tool for survivable C+L+S MB networks

This section introduces the GNPy tool and its capabilities in Section 3.1. The RMSA algorithm used in this work is then presented in Section 3.2 and the main changes made to the RMSA algorithm of the GNPy tool to incorporate optical protection are highlighted in Section 3.3. The outputs of the RMSA simulator are defined in Section 3.4.

3.1. GNPy tool

The GNPy tool is an open-source, community-developed library used for optical network planning and analysis [19]. It is also highly customizable, enabling users to define building blocks, parameters for fine-tuning physical models, and physical and logical network topologies [19] using a Javascript Object Notation (JSON) or Excel file. The basic use of the GNPy tool is shown in Fig. 2. It starts by loading the user-defined files and building a new virtual network instance, followed by the path computation and lastly propagating the signal through the path, using the RamanSolver and NliSolver modules to compute the path quality of transmission, through the generalized Gaussian noise (GGN) model.

The GNPy version 2.8.0, released on the 4th of December 2023 is used in this work.

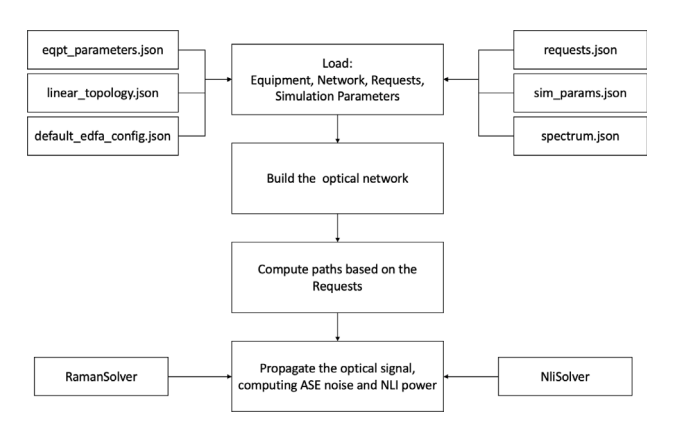


Fig. 2. Flowchart of the GNPy tool basic use.

3.2. GNPy-based RMSA simulator without protection

This subsection presents the GNPy-based simulator used in this work to solve the RMSA problem without protection, whose flowchart is illustrated in Fig. 3. It is based on the function <code>path_requests_run()</code> which encompasses all the steps presented in Fig. 2 and can be found on the <code>cli_examples.py</code> file, implemented in the GNPy tool [19].

The simulator follows the statistical network assessment process (SNAP) model [21], which considers incremental traffic and is implemented in four steps as described in Fig. 3. The SNAP model uses a Monte Carlo (MC) simulation method with a predefined number of MC iterations (N_{MC}) and a predefined number of requests per iteration (N_{req}) that depends on the studied scenario. The four main steps are: (1) build the virtual instance of the network, (2) group and aggregate the requests, (3) find a path, assign the modulation format and compute the path OSNR, and (4) spectrum assignment. After the last MC iteration, several simulator outputs are used to analyze the RMSA results.

In the first step, a new virtual instance of the network in each MC iteration is created and the simulator loads the JSON files provided by the user to build the network, i.e. all the files presented in Fig. 2. Note that to write the request.json file, we have developed a function to dynamically generate the requests based on the total number of requests. A request is defined by at least three features: the source node, the destination node, and the request capacity to be transported. Based on the network topology, this newly developed function generates N_{req} requests with a uniform distribution between the network nodes, unless a different distribution is specified by the user. The requests capacity is also chosen from a predefined set of equiprobable capacities unless otherwise specified.

After building the network, the second step of the <code>path_requests_rum()</code> function is only performed for static network traffic scenarios. In this case, the GNPy tool can use the <code>requests_aggregation()</code> function, as shown in Fig. 3 to aggregate requests that share the same characteristics. As, in this work, we are studying an incremental traffic network scenario, in which the requests are not known previously, we will not consider request aggregation.

The third step, named Find path, compute OSNR and assign modulation format and highlighted with more detail in Fig. 4, computes the path for each one of the requests, in the Find propagation path block shown in Fig. 4. It also ensures that a predefined safety margin is accomplished in each path, in the Propagate block in Fig. 4. The Find propagation path block uses the function <code>compute_path_dsjctn()</code> that can be programmed to give just the shortest path, or to give several paths between the selected source and destination nodes, including disjoint paths [22]. This function will not return a feasible path, <code>i.e.</code>, the request will be blocked (blocking conditions are highlighted in the flowchart by the red boxes), if there is no physical path between the selected source and destination nodes (NO_PATH condition in Fig. 4) or if there

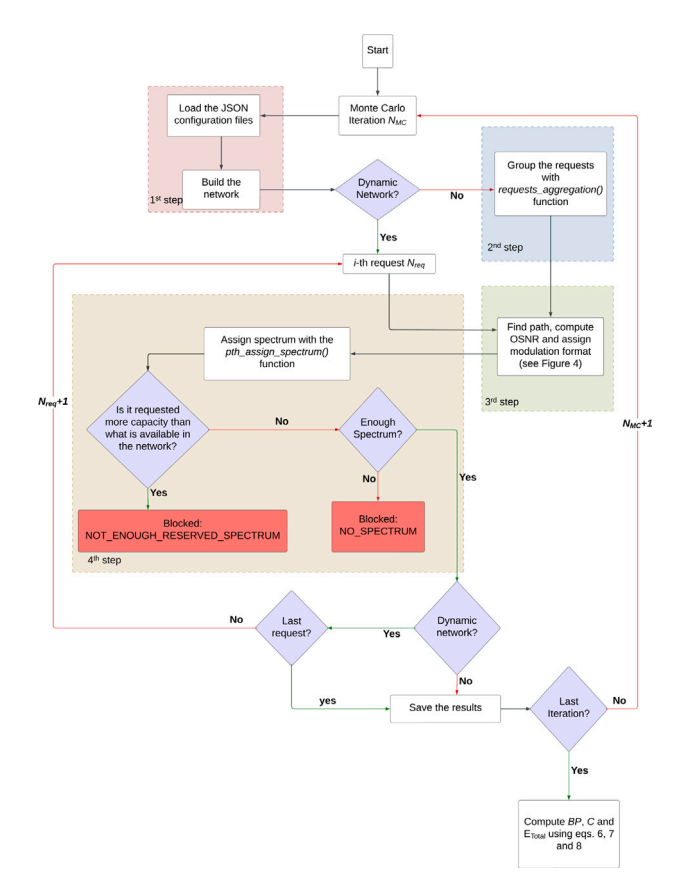


Fig. 3. Flowchart of the RMSA algorithm implemented in the GNPy tool in the path requests run() function.

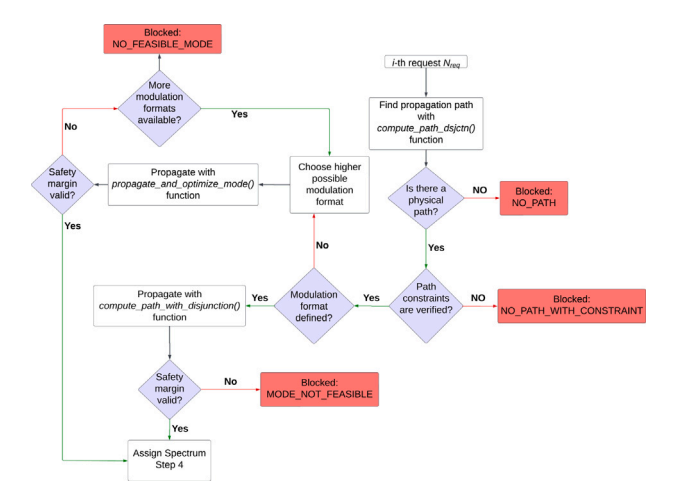


Fig. 4. Flowchart of the Find path, compute OSNR and assign modulation format step (step 3) of the RMSA algorithm shown in Fig. 3.

is no path that can provide the requested path constraints, $\it e.g.$, find two disjoint paths (NO_PATH_WITH_CONSTRAINT in Fig. 4).

After path computation, the Propagate block in Fig. 4 ensures that each path provides the defined safety margin for that specific request. If the request specifies the signal modulation format, this block uses the *compute_path_with_disjunction()* function, otherwise it uses the *propagate_and_optimize_mode()* function. In both functions, the generalized signal-to-noise ratio (GSNR) of each path is computed using [19],

$$GSNR = \frac{p_{ch}}{p_{ASE} + p_{NLI}} \tag{1}$$

where p_{ch} is the optical channel power, p_{ASE} and p_{NLI} are, respectively, the channel amplified spontaneous emissions (ASE) noise and NLI noise powers, evaluated at the receiver.

The ASE noise power as a function of the frequency, f, is given by,

$$p_{ASE}(f) = hf NF(f)G(f)B_{ref}$$
(2)

where h is the Planck constant, NF(f) and G(f) are, respectively, the noise figure and the amplifier gain, that include ASE noise inflation [10], and B_{ref} is the reference bandwidth, considered to be the same as the symbol rate.

To compute the NLI noise power, a simplified version of the GGN model, known in the literature as the ISRS-GN model, is used in the RMSA algorithm, since it is not practical to use the GGN model presented in the tool to perform computations in large network simulations [23]. With the ISRS-GN model, we were able to accomplish very similar results with a computational time reduction of approximately 8000 times, as was also shown in [23].

The NLI noise power, p_{NLI} , is given by [10],

$$p_{NLI}(f_i) = \eta(f_i)p_{ch}^3(f_i) \tag{3}$$

with the NLI coefficient $\eta(f_i)$ given by,

$$\eta(f_i) \approx \sum_{i=1}^{n} \left[\frac{p_{ch,j}}{p_{ch}} \right]^2 \cdot \left[\eta_{SPM,j}(f_i) n^{\epsilon} + \eta_{XPM,j}(f_i) \right] \tag{4}$$

where $\eta_{SPM,j}(f_i)$ is the self-phase modulation coefficient of the channel at frequency f_i in the jth span, defined in [10]; $\eta_{XPM,j}(f_i)$ is the crossphase modulation coefficient, at frequency f_i in the jth span, also defined in [10]; $p_{ch,j}$ is the channel launch power in jth span; n is the number of spans along an optical path; and ϵ is the coherence factor, which allows taking into account the NLI coherent accumulation along multiple spans. Typical network planning, as the one performed in this work, usually assumes incoherent accumulation of NLI, because of the different lengths of spans on each link [3,24].

The modulation format used in Eq. (1) is assigned to a particular path if it verifies the following condition:

$$GSNR - ROSNR > SM \tag{5}$$

where SM is the defined safety margin and ROSNR is the required optical signal-to-noise ratio.

If the defined SM is not met and a specific modulation format has been set to that request, then the request is considered blocked (MODE_NOT_FEASIBLE in Fig. 4). Otherwise, if the defined SM is not met, but a specific modulation is not defined (the scenario used in this work), then a lower modulation format is tried (note that the higher possible modulation format is always tried first). If none of the modulation formats are able to meet the defined SM, then that request is blocked (NO_FEASIBLE_MODE in Fig. 4). The simulator tries to solve this issue by splitting a request in multiple requests (not shown in Fig. 4), if the requested capacity is greater than the maximum capacity allowed by the modulation format. For example, if the requested capacity is 400 Gbit/s, but the assigned modulation format is only capable of transmitting 200 Gbit/s, the request will be split in two.

In this step, two other blocking conditions may arise (not shown in Fig. 4): NO_COMPUTED_SNR, if by any reason the system was not able to compute a GSNR for a given path, NO_FEASIBLE_BAUDRATE_WITH_SPACING, if the request specifies a minimum spacing and none of the available modulation formats respects the specified spacing.

The fourth step, in Fig. 4, assigns a slice of spectrum to each particular request. In the assignment process, the Frequency Slots (FSs), each with a width of 12.5 GHz (as defined in the standards [25]), allocated to a request must be contiguous and continuous [20], *i.e.*, the FSs must be adjacent in frequency and the same FSs must be used consistently across every link of the path. For example, if a request uses an optical channel with 75 GHz, it means that 6 contiguous and continuous FSs in every link of the path must be assigned to that request. If these

conditions cannot be met, than the request is blocked (NOT_ENOUGH _RESERVED_SPECTRUM or NO_SPECTRUM conditions shown in Fig. 4). The FSs are assigned using the First Fit (FF) strategy [20], starting with L-band channels, which typically have the highest GSNRs [23], then C-band channels, and finally S-band channels (with the worst GSNRs).

In the fourth step, a strategy to reduce the spare capacity, defined as the difference between the requested capacity and the capacity provided by the modulation format, was also implemented as in [8]. The strategy works like this: before assigning new FSs, the simulator checks if there is any request with the same path that has spare capacity and if so, the request uses that capacity, saving FSs for allocation to new requests. For example, if a 200 Gbit/s request is assigned to a modulation format that allows a capacity of 400 Gbit/s, it means that there is a spare capacity of 200 Gbit/s that can be used later by other requests.

3.3. GNPy-based RMSA simulator with protection

When client-side dedicated protection is considered, there are a number of differences regarding the RMSA algorithm just presented in Section 3.2 that does not consider protection.

In the first step of Fig. 3, when protection is considered, for every protected request an exact copy of that request is generated and marked as disjoint — this is another feature of a request alongside the definitions of the source node, destination node and capacity. In our simulator, as in a real scenario, not every request requires protection, for example, a 50% protection level means that only half of the requests require protection. To assess whether a request has protection or not, a deterministic rule has been followed, for simplicity. The service level agreement of the request, another request feature, indicates whether a request must have a protection path or not [20].

In the third step, when protection is considered, the routing in a RMSA algorithm becomes more complex, since it needs to find a path not only for service, but also for protection, and these two paths must be completely disjoint (the two demands must not share any link or node, except the source and destination nodes) [20]. In this case, the function <code>compute_path_dsjctn()</code> computes both service and protection paths, yielding the same results as the <code>Suurballe</code> algorithm [26].

Regarding the blocking conditions shown in Fig. 3 they are all applied when protection is used. But it is also important to emphasize that when protection is considered, as the service and protection requests are handled at the same time, if one of them is blocked, the other is also blocked.

3.4. Simulator outputs

The simulator tries to assign the total number of requests (N_{req}) and after the last MC iteration ends, the results are analyzed to obtain the total network capacity for a predetermined BP, as shown in Fig. 3.

The average BP is computed by averaging all BPs obtained per MC iteration. The BP per MC iteration, BP_i , is obtained by dividing the sum of blocked requests on the ith iteration ($N_{blocked,requests,i}$) by the total number of processed requests in the ith iteration ($N_{total,requests,i}$), up to a certain targeted BP, like in [8], and is given by,

$$BP = \frac{\sum_{i=1}^{N_{MC}} BP_i}{N_{MC}} = \frac{\sum_{i=1}^{N_{MC}} \frac{N_{blocked,requests,i}}{N_{total,requests,i}}}{N_{MC}}$$
(6)

The transported network capacity (in Tbit/s) is computed by summing the capacity of the provisioned requests per MC iteration ($C_{request,j,i}$), like in [8] as,

$$C_{total} = \frac{\sum_{i=1}^{N_{MC}} C_{total,i}}{N_{MC}} = \frac{\sum_{i=1}^{N_{MC}} \sum_{j=1}^{N_{req}} C_{request,j,i}}{N_{MC}}$$
(7)

where $C_{total,i}$ is the total transported capacity per MC iteration.

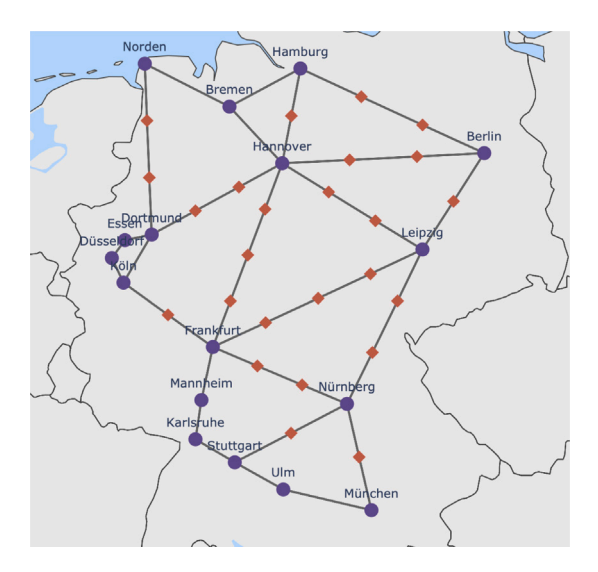


Fig. 5. Germany network topology with 17 nodes. *Source:* Figure taken from [27].

In this work, we will also compute the total network consumed energy per Tbit (in dBJpTbit), as in [8] by using

$$\begin{split} E_{total} &= 10 \log_{10} \left(\frac{\sum_{i=1}^{N_{MC}} E_{Total,i}}{N_{MC}} \right) = \\ &= 10 \log_{10} \left(\frac{\sum_{i=1}^{N_{MC}} \frac{2 \times \sum_{j=1}^{N_{req}} P_{Trx,i,j} + N_{OA} \times P_{OA} + N_{WSS} \times P_{WSS}}{C_{total,i}}}{N_{MC}} \right) \end{split} \tag{8}$$

where $E_{Total,i}$ is the total energy per Tbit consumed by the network in the ith MC iteration and calculated by summing the power consumption of all requests in the ith iteration, divided by the total transported capacity obtained in the ith iteration, $C_{total,i}$. The power consumption of each transceiver for request j and iteration i is denoted as $P_{Trx,i,j}$. In Eq. (8), the multiplicative factor 2 before the sum relative to j, considers both the transceivers at source and destination. N_{OA} and N_{WSS} are, respectively, the total number of optical amplifiers (one optical amplifier per band is considered) and wavelength selective switches (WSSs) in the network. P_{OA} and P_{WSS} represent, respectively, the power consumption of an optical amplifier per band and the power consumption of a single WSS.

4. Simulator parameters and validation

In this section, we start by describing the simulation parameters and then perform a validation of the simulator by, comparing our results with results from [21], for a scenario without protection.

4.1. Simulation parameters

In this subsection, the simulation parameters considered for this work are presented. Regarding the network topology, we have used the German network, available in [27] and shown in Fig. 5.

The German network topology has 17 nodes. In this work, we consider that each C+L+S ROADM node has a route and select (R&S) baseline architecture [11], as shown in Fig. 6. Each node has a band multiplexer/demultiplexer in each direction and 2 WSSs per direction and per band. Nowadays, this is the most common MB node, where the traffic is routed separately in each band and switching between bands is not allowed [11]. It is considered that each node imposes a loss of 18 dB [21], that is perfectly compensated by a booster amplifier. The

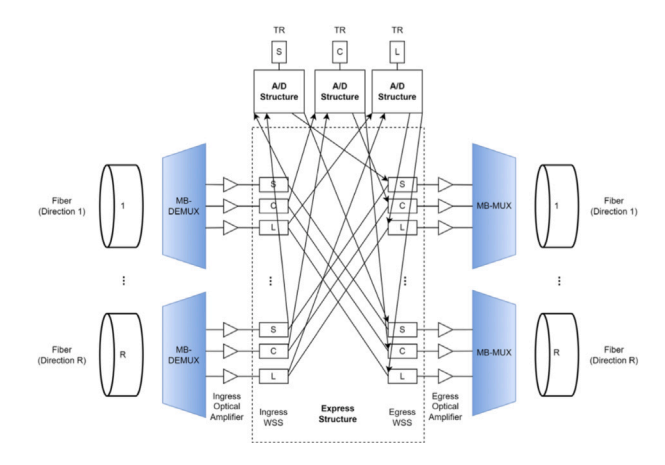


Fig. 6. Baseline R-degree R&S C+L+S MB ROADM node architecture (TR = transceiver, A/D = add/drop, MUX = multiplexer, DEMUX = demultiplexer).

Source: Figure taken from [11].

average node degree is 3.25 and the total number of links is 26, with an average distance of 168.4 km. The node with the highest degree is Hannover, with 6 directions, while the lowest degree is 2, in several cities such as Dortmund, Norden, and Essen, among others. The shortest link is between the cities of Düsseldorf and Essen with 37 km, while the longest link is between the cities of Frankfurt and Leipzig with 352.6 km. In Fig. 5, each orange diamond represents an in-line amplifier (the network has a total of 25 per band) designed to perfectly compensate for the span loss.

Table 1 shows the physical layer parameters used in our simulations and Table 2 presents the three modulation formats used in the simulations [3,28]. The minimum ROSNR is taken from [8], and a 2 dB SM to account for additional OSNR degradation is considered. Connector losses are considered negligible. It should be noticed that using the modulation formats presented in Table 2, each modulation format will always require 6 FSs that occupy 75 GHz, the bandwidth necessary to accommodate a 64 GBd signal. The transceiver power consumption values for each modulation format are taken from [8]. For simplicity, the power of an amplifier, independently of the band, is considered to be $P_{OA}=15$ W, however, in a real scenario, the S-band amplifiers tend to consume more power [18]. The WSSs inside the ROADM node are assumed to be 1×9 and to consume $P_{WSS}=12$ W each [18]. These assumptions are assumed for simplicity, since in real scenario, their power consumption also depends on the band.

We consider 100 MC iterations ($N_{MC}=100$) in each simulation, while the number of requests N_{req} varies with the protection level, to ensure that enough requests are considered for the results to stabilize. Regarding the request generation, we used the SNAP model, with the requests being randomly generated with a uniform distribution across all network nodes. The capacity of each request is, 100 Gbit/s, 200 Gbit/s, or 400 Gbit/s, and is also chosen randomly with equal probability for each request.

4.2. Simulator validations

We have performed an RMSA validation by comparison with the results from [21], for the German network topology. In this scenario, the bandwidth used was the C-band with 4 THz, and the requests may only be 100 Gbit/s or 200 Gbit/s. No protection is considered.

Our simulator has some differences when compared to the one considered in [21]: (1) in [21], the k_{max} -best-OSNR algorithm (equivalent to the k-shortest path algorithm, but using the OSNR as metric instead of the path length) is used as the routing algorithm with $k_{max} = 50$, while in this work, we have used only $k_{max} = 1$; (2) we have implemented the re-utilization of spare capacity, while in [21] this

Table 1 Simulation physical parameters.

Parameter	Value	Parameter	Value
Loss coefficient (α) [dB/km]	0.2	C-L-band [THz]	185–195.07
Dispersion slope (S) [ps/nm ² /km]	0	C-L-S-Band [THz]	185-201.4
Dispersion (D) [ps/nm/km]	17	Launch power [dBm]	0
Nonlinear coefficient (γ) [1/W/km]	1.27	Connector In losses [dB]	0
Effective area (A_{eff}) [μ m ²]	80	Connector Out losses [dB]	0

Table 2
Transceiver modulation formats defined for the simulations.

Modulation format	Bit rate [Gbit/s]	Baud rate [GBd]	Minimum ROSNR [dB]	Power [W]
16QAM	400	64	16.9	20
8QAM	300	64	13.9	18
QPSK	200	64	8.9	16

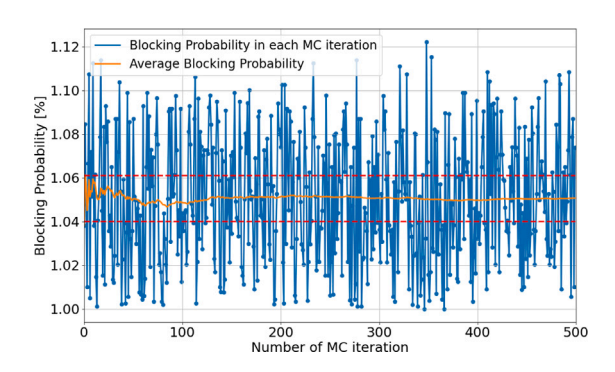


Fig. 7. BP as a function of the number of MC iteration for a target BP of 1%.

is not implemented, and (3) in [21], the authors use the GN model, developed for estimating the NLI in the C-band, which does not take into account the ISRS effect and is computationally much faster than the GGN model [23,29]. In this work, we use the ISRS-GN model which, according to our validation, leads to very similar results in comparison with the GGN model and is computationally much faster, as already referred in the previous section.

We have observed that our simulator always stabilizes at a target BP, if enough requests are provided, as it can be observed in Fig. 7, where it is shown the BP and the average BP as a function of the number of MC iterations for this validation scenario, with a target BP of 1% and a total of 500 MC iterations. From Fig. 7, it can be concluded that the average BP tends to the target BP of 1%, soon after the first MC iteration.

Fig. 8 shows the total transported capacity per iteration (blue line) as well as the average network capacity (orange line) in Tbit/s, as a function of the number of MC iterations, for the target BPs of 1% and 10%. The horizontal lines in red correspond to capacity thresholds that are defined at 2 Tbit/s above and below the average capacity obtained at the last iteration, to establish a criterion for network capacity stabilization.

As we can observe in Fig. 8, the transported capacity has stabilized for both BPs in the first 10 MC iterations, respectively, reaching 130.7 Tbit/s and 188.7 Tbit/s after 500 MC iterations. These values are 15.7% less and 2% more (which is a very approximated result) capacity than the values presented in [21], which can be considered acceptable results due to the simulators differences. The use of k=1 leads to lower transported capacities for lower BPs, since there are no other available paths when the first one is blocked, and for higher BPs, the difference in transported capacity is compensated by the reutilization of spectrum due to the implementation of the strategy for spare capacity reduction. These results also show that with $k_{max}=1$, there is no requirement to perform a high number of MC iterations to obtain stabilized values of the average network capacity, such as the 5000 iterations considered in [21]. It should also be noticed that the most assigned modulation format in our simulations is the 16QAM, just like in [21].

5. Case study: The German network

This section presents and discusses the results obtained with our RMSA simulator, regarding the transported and spare capacities, as well as the energy consumption per Tbit, considering the MB C+L-and C+L+S-bands, using various levels of protection (no protection, 25%, 50%, 75%, and full protection), for the German network scenario. For the fully protected scenario, in the C+L+S-band, the impact of the traffic pattern is also analyzed.

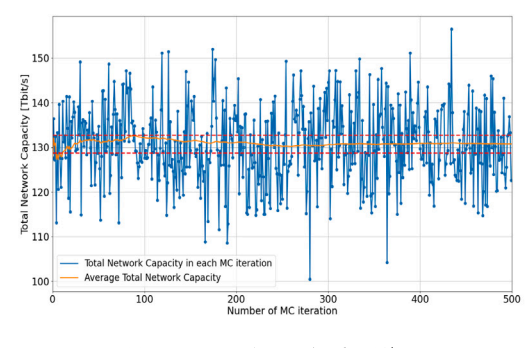
5.1. Impact of the path protection level on network performance

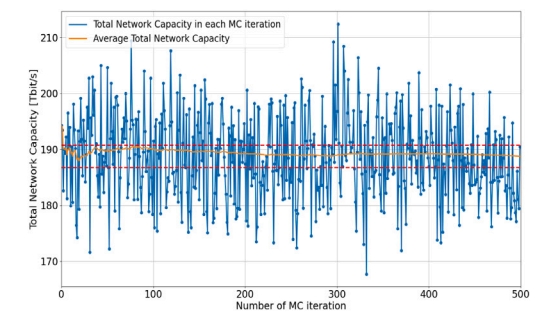
In this subsection, the results of the RMSA simulations concerning the German network performance are presented. In particular, results showing the average transported capacity, the percentage of spare capacity in relation to the transported capacity, and the energy consumption per Tbit, considering the transceiver, optical amplifier and WSS consumptions are discussed for five different protection levels. All results shown are obtained after averaging the results estimated for 100 MC iterations.

Fig. 9 represents the transported capacity as a function of the protection level for 1% and 10% BPs. The results from Fig. 9 show that, as expected, the transported capacity decreases with the level of protection, since, by increasing the level of protection, the number of protection paths (that do not impact the transported capacity) increases. We observe that, for the 1% BP, in the C+L+S-band, on average, increasing the protection level by 25%, leads to a decrease in transported capacity of approximately 11% (except when going from fully unprotected to 25% protected, with a sharper decrease of 38%, and when going from 75% protection to the fully protected scenario, where the transported capacities become very similar). After the 75% protection level, our results seem to have stabilized, with the transported capacity reaching approximately 150 Tbit/s. For the 10% BP, higher transported capacities are reached for all protection levels, in comparison with the 1% BP scenario due to having more requests provisioned, and the transported capacity has a similar behavior with the increase of protection to the one found for the 1% BP.

Fig. 10 shows the BPs as a function of the average transported capacities, for the C+L and C+L+S band scenarios, for no protection, 50%, and 100% (full) protection levels. We observe that using the C+L+S-band leads to a 60% increase in the transported capacity, when compared to the use of the C+L-band only, due to the wider bandwidth available. As the BP is increased, we observe an increase in the transported capacity due to the higher number of provisioned requests and spectrum reuse, which is most noticeable in the unprotected scenarios. Fig. 10 also shows that the unprotected scenario leads to a higher transported capacity since there are no FSs allocated for protection.

Fig. 11 shows the percentage of spare capacity as a function of the protection level, for the C+L+S band and 1% and 10% BPs. As we can observe, an increase of 25% in the protection level leads to

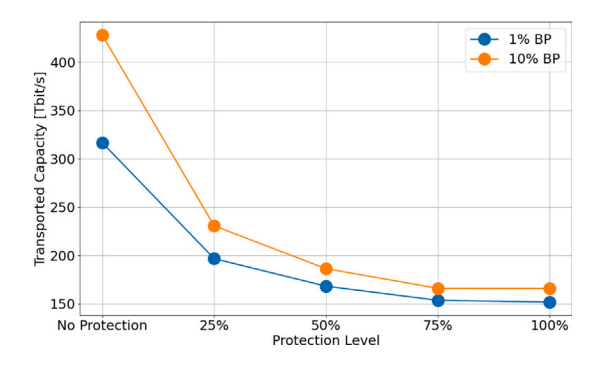




(a) Transported capacity for 1% BP

(b) Transported capacity for 10% BP

Fig. 8. Total network capacity per MC iteration and its average for 100 iterations for the BPs of 1%, and 10%, for the German network topology.



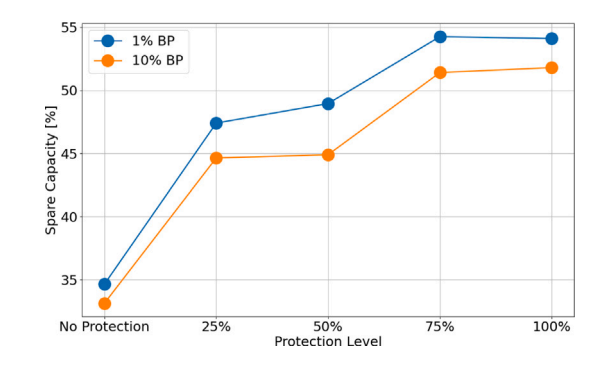
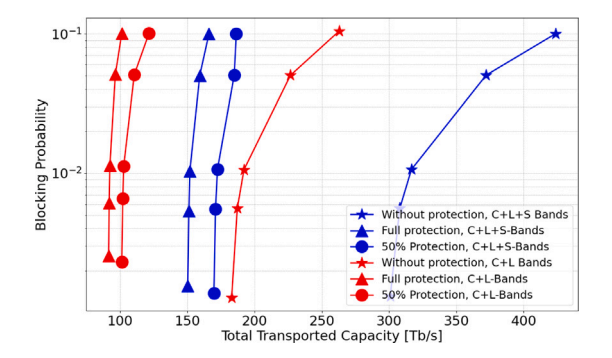


Fig. 9. Average network transported capacity for the BPs of 1% and 10%, as a function of the protection level, for the C+L+S MB scenario.

Fig. 11. Average network spare capacity for the BPs of 1% and 10%, as a function of the protection level, for the C+L+S MB scenario.



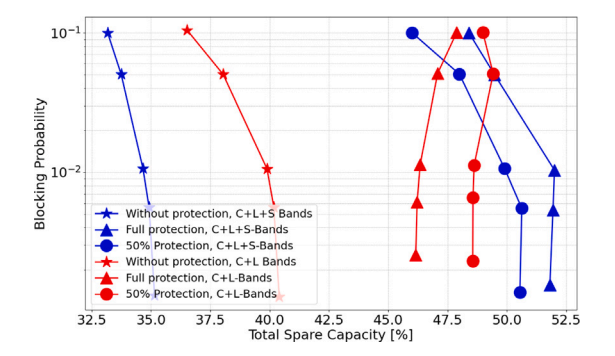


Fig. 10. BP as a function of the transported capacity for the two MB cases, C+L-, and C+L+S-bands.

Fig. 12. BP as a function of the spare capacity for the two MB cases, C+L-, and C+L+S-bands.

an increase of about 4% in the percentage of spare capacity, except from no protection to the first 25% protection increase, where the percentage of spare capacity increases more abruptly by 12.8% and near the 100% protection level, where the percentage of spare capacity tends to stabilize between 50% and 55%. We observe an increase of spare capacity with the protection level increase, since by having more protected requests, more paths are provisioned, and more spare capacity can exist, as we are generating spare capacity not only in the service path, but also in the protected path.

Fig. 12 shows the BPs as a function of the percentage of spare capacity, for the C+L and C+L+S scenarios. It can be observed that, when there are protected requests, the C+L+S scenario, shows higher percentages of spare capacity, and lower percentages when there are no protected requests. For the fully protected scenario, we observe that using the C+L+S-band leads to approximately 6% more spare capacity at the 1% BP when compared to the C+L-band scenario, and nearly the same spare capacity at the 10% BP. In the C+L+S scenario, higher BPs show less spare capacity, as there are more provisioned requests

available for reusing, leading to a reduction in spare capacity. We can also observe, for the C+L+S scenario that, as concluded in Fig. 11, higher protection levels lead to higher spare capacities due to the higher number of protection paths. Another observation comes from the fact that in the C+L band scenario there is more spare capacity at the 50% protection level, than in the full protection level, which is just the opposite behavior found for the C+L+S scenario. This is explained by the reutilization of spare capacity — in the C+L+S scenario, since there are more provisioned paths, we observe approximately 5% more reutilization of the spare capacity compared to the C+L scenario, leading to this unexpected behavior.

Fig. 13 shows the energy consumption per Tbit as a function of the protection level, for the C+L+S band and 1% and 10% BPs. It shows that a 25% protection level increase results approximately in a 1 dBJpTbit energy consumption increase. The energy consumption per Tbit stabilizes between 25.5 and 26 dBJpTbit, for the 75% protection level. The observed increase can be attributed to the fact that, despite, the utilization of a protection path inevitably results in the consumption

Table 3

Average transported capacities with different traffic patterns for 1% and 10% BPs, for the German network topology.

Blocking	Uniform	6 nodes	6 nodes	3 nodes	9 nodes
Probability	Distribution	2 times more probable	4 times more probable	2 times more probable	2 times more probable
1%	152 Tbit/s	152 Tbit/s	138.4 Tbit/s	152.7 Tbit/s	146.5 Tbit/s
10%	166 Tbit/s	166 Tbit/s	151.5 Tbit/s	171.6 Tbit/s	157.9 Tbit/s

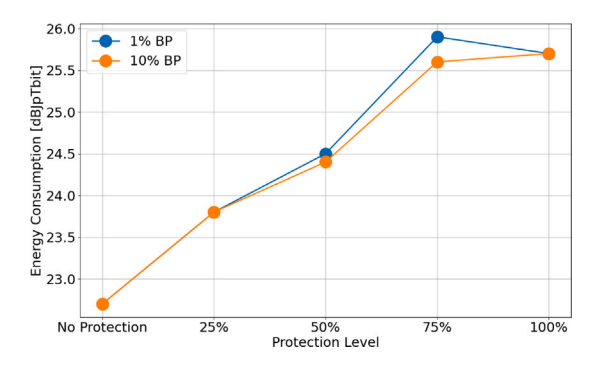


Fig. 13. Average network energy consumption for the BPs of 1% and 10%, as a function of the protection level, for the C+L+S MB scenario.

of more energy, the protected capacity is not included in the transported capacity, which effectively leads to an increase in the average energy consumption per Tbit. We can observe a very similar energy consumption per Tbit behavior for the two BPs, with an almost linear increase until the 75% protection level is reached, since provisioning more requests leads to higher consumptions and also leads to higher transported capacities. For protection levels above or equal to 50%, the energy consumption per Tbit obtained for the BPs of 1% and 10% starts to differ. This slight difference is attributed to the higher reutilization of the spectrum found for the 10% BP, which leads to a higher transported capacity, while maintaining the same energy consumption, ultimately reducing the energy consumption per Tbit.

We have also concluded in our work that nearly the same energy per Tbit is consumed when using the C+L+S MB scenario or the C+L scenario, despite the C+L+S-band allows higher transported capacities. Since 98% of the energy is consumed by the transceivers, when adding the S-band, we observe an increase in energy consumption proportionally to the increase in transported capacity, leading to similar average energy consumptions per Tbit on both MB scenarios.

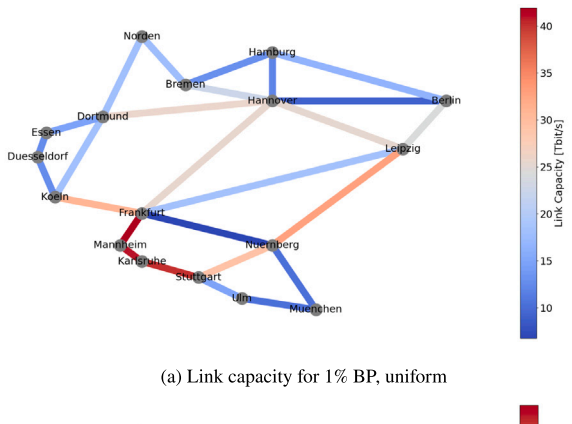
Moreover, regarding the modulation formats assigned, we have observed that, in all simulations, all requests have been provisioned with the 16QAM for the German network topology, due to short network links.

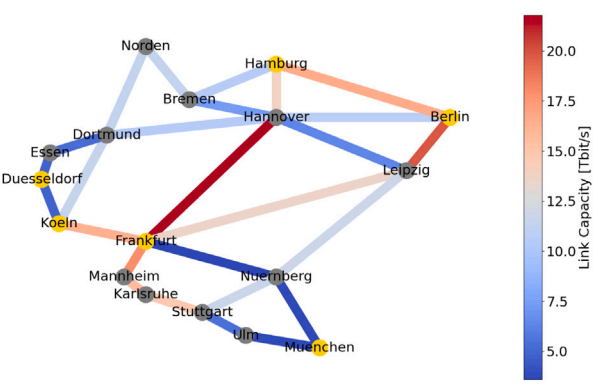
A final remark on the simulation computational time: it is highly dependent on the number of requests and tends to increase by five minutes per 25% increase in the protection level. We have also observed that 81% of this time is consumed with the path OSNR computations.

5.2. Impact of the traffic pattern on network performance

In this subsection, we present several RMSA simulations on the C+L+S fully protected scenario, with different traffic distributions.

Table 3 shows the transported capacities when using different traffic patterns. Besides the uniform traffic scenario the following scenarios are considered: 6 nodes with 2 times the probability of being chosen (so 25% traffic is between large nodes, 25% traffic is between small nodes, and 50% traffic is between large and small nodes); 6 nodes with 4 times the probability of being chosen (so 64% traffic is between large nodes, 4% traffic is between small nodes and 32% traffic is between large and small nodes); the three most populated (Munchen, Hamburg, and Berlin) cities with 2 times more probability (so 9% traffic is between large nodes, 49% traffic is between small nodes and 42% traffic is





(b) Link capacity for 1% BP, non-uniform

Fig. 14. Average link capacity in the German network, for a 1% BP, with (a) uniform distribution and (b) non-uniform distribution.

between large and small nodes); and 9 (Essen, Dortmund, Stuttgart plus the ones highlighted in yellow in Fig. 14(b)) nodes with 2 times the probability of being chosen (so 48% traffic is between large nodes, 9% traffic is between small nodes and 43% traffic is between large and small nodes).

From Table 3, we conclude that the traffic pattern has a small effect on the transported capacity, a maximum variation of 9.2% when compared to the uniform distribution scenario is observed, when 64% of the traffic is between large nodes, 4% of the traffic is between small nodes and 32% of the traffic is between large and small nodes. Regarding the spare capacity (not shown in Table 3), we observe that it reaches 53.3% for the 1% BP and 55% for the 10% BP, which are very close results to the ones obtained for the uniform distribution. We have also seen that the energy consumption per Tbit remains constant at 25.6 dBJpTbit for all the considered traffic scenarios, and is very similar to the one obtained for the uniform distribution.

Fig. 14 shows the link utilization in terms of capacity, for (a) the uniform scenario, and (b) the non-uniform scenario along the German network topology (6 nodes with 4 times the probability of being chosen - highlighted in yellow). As observed in Fig. 14, when changing the node distribution, there is a difference in the links utilization, although, as shown in Table 3, the total network transported capacity does not change much. Most notably, we observe less utilization in shorter links, for example, on the network's west side, such as the ones from Frankfurt to Stuttgart, and a higher link utilization on the longer links such as

Hannover–Frankfurt, Frankfurt–Leipzig, and Hamburg–Berlin, due to the new traffic pattern leading to a higher utilization of longer links.

6. Conclusions

In this work, we have developed a GNPy-based RMSA simulator, to evaluate the impact of the level of protection on the transported and spare capacities, as well as on the energy consumption for the C+L- and C+L+S-band scenarios. We have studied five different protection levels on the German network topology, ranging from no requests protected to fully protected requests.

We have seen that an increase of 25% in the protection level leads to about an 11% decrease in the transported capacity, a 4% increase in the spare capacity, and a 1 dBJpTbit increase in energy consumption per Tbit. Both transported and spare capacities tend to stabilize when the protection level becomes higher than 50%. The energy consumption grows linearly with the protection level, up to the 75% level, and becomes nearly constant for higher protection levels.

We have concluded that the highest capacity is transported in the unprotected scenario, reaching 316.6 Tbit/s for a 1% BP, while the lowest transported capacity is obtained in the fully protected scenario, reaching 151.9 Tbit/s, which is less than half the capacity of the unprotected scenario. As the protection level increases, the transported capacity is reduced, since more bandwidth is being used for protection. Regarding the percentage of spare capacity, the lowest values are found in the unprotected scenario, with 34.6% at 1% BP, and the highest values of 55.4% are found in the fully protected scenario at 10% BP.

The C+L+S MB scenario leads to higher transported capacities due to the wider bandwidth when compared to the C+L scenario, with a small increase in the spare capacity. Despite the higher transported capacity, there is no difference in the energy consumption per Tbit, since 98% of the energy is consumed by the transceivers.

Our results show that the traffic pattern can influence the total average transported capacity, with a maximum variation of 9.2%. However, the network average energy consumption and spare capacity are not practically affected by changes in the traffic pattern.

CRediT authorship contribution statement

Rodrigo Guerreiro: Writing – original draft, Visualization, Validation, Software, Methodology, Investigation, Formal analysis, Data curation. Luís Cancela: Writing – review & editing, Visualization, Validation, Supervision, Project administration, Methodology, Investigation, Formal analysis, Data curation, Conceptualization. João Rebola: Writing – review & editing, Visualization, Validation, Supervision, Project administration, Methodology, Investigation, Formal analysis, Data curation, Conceptualization.

Declaration of competing interest

The authors declare that they have no known competing financial interests or personal relationships that could have appeared to influence the work reported in this paper.

Acknowledgments

This work was supported in part by Fundação para a Ciência e Tecnologia/Ministério da Ciência, Tecnologia e Ensino Superior (FCT/MCTES) under Project UIDB/50008/2020.

Data availability

The authors are unable or have chosen not to specify which data has been used.

References

- Ericsson, Mobile data traffic outlook, 2023, URL: https://www.ericsson.com/en/ reports-and-papers/mobility-report/dataforecasts/mobile-traffic-forecast.
- [2] N. Deng, L. Zong, H. Jiang, Y. Duan, K. Zhang, Challenges and enabling technologies for multi-band MakeUppercaseWDM optical networks, J. Lightwave Technol. 40 (11) (2022) 3385–3394.
- [3] M. Mehrabi, H. Beyranvand, M. Emadi, Multi-band elastic optical networks: Inter-channel stimulated MakeUppercaseRaman scattering-aware routing, modulation level and spectrum assignment, J. Lightwave Technol. 39 (11) (2021) 3360–3370.
- [4] D. Uzunidis, E. Kosmatos, C. Matrakidis, A. Stavdas, A. Lord, Strategies for upgrading an operator's backbone network beyond the MakeUppercaseC-band: Towards multi-band optical networks. IEEE Photonics J. 13 (2) (2021) 1–18.
- [5] Infinera, FlexILS series open optical line system, 2023, URL: https://www.infinera.com/products/infinera-flexible-grid-line-system-flexils/.
- [6] M. Cantono, R. Schmogrow, M. Newland, V. Vusirikala, T. Hofmeister, Opportunities and challenges of MakeUppercaseC+L transmission systems, J. Lightwave Technol. 38 (5) (2020) 1050-1060.
- [7] B. Puttnam, R. Luis, I. Phillips, M. Tan, A. Donodin, D. Pratiwi, L. Dallachiesa, Y. Huang, M. Mazur, N.K. Fontaine, H. Chen, D. Chung, V. Ho, D. Orsuti, B. Boriboon, G. Rademacher, L. Palmieri, R. Man, R. Ryf, D.T. Neilson, W. Forysiak, H. Furukawa, 402 Tb/s GMI data-rate OESCLU-band transmission, in: 2024 Optical Fiber Communications Conference and Exhibition, OFC, 2024, pp. 1.2
- [8] R. Sadeghi, B. Correia, A. Souza, N. Costa, J. Pedro, A. Napoli, V. Curri, Transparent vs translucent multi-band optical networking: Capacity and energy analyses, J. Lightwave Technol. 40 (11) (2022) 3486–3498.
- [9] A. Souza, B. Correia, N. Costa, J. Pedro, J. Pires, Accurate and scalable quality of transmission estimation for wideband optical systems, in: 2021 IEEE 26th International Workshop on Computer Aided Modeling and Design of Communication Links and Networks, CAMAD, 2021, http://dx.doi.org/10.1109/CAMAD52502. 2021.9617794.
- [10] D. Semrau, R. Killey, P. Bayvel, A closed-form approximation of the Gaussian noise model in the presence of inter-channel stimulated Raman scattering, J. Lightwave Technol. 37 (9) (2019) 1924–1936.
- [11] J. O'Ramos, L. Cancela, J. Rebola, Influence of the ROADM architecture on the cost-per-bit in C+L+S multi-band optical networks, in: 2023 23rd International Conference on Transparent Optical Networks, ICTON, 2023, http://dx.doi.org/ 10.1109/ICTON59386.2023.10207552.
- [12] A. Eira, J. Pedro, On the comparative efficiency of next-generation coherent interfaces for survivable network design, in: 2021 17th International Conference on the Design of Reliable Communication Networks, DRCN, 2021, http://dx. doi.org/10.1109/DRCN51631.2021.9477395.
- [13] G. Shen, H. Guo, S.K. Bose, Survivable elastic optical networks: Survey and perspective, Photonics Netw. Commun. 31 (1) (2016) 71–87.
- [14] Z. Luo, S. Yin, L. Zhao, Z. Wang, W. Zhang, L. Jiang, S. Huang, Survivable routing, spectrum, core and band assignment in multi-band space division multiplexing elastic optical networks, J. Lightwave Technol. 40 (11) (2022) 3442–3455.
- [15] S. Hosseini, I. de Miguel, Ó.G. de Dios, N. Merayo, J.P. Fernández-Palacios, R.J. Durán Barroso, Dynamic restoration assessment in partially upgraded networks from the C to the C+L bands, in: 2024 20th International Conference on the Design of Reliable Communication Networks, DRCN, 2024, pp. 123–128, http://dx.doi.org/10.1109/DRCN60692.2024.10539152.
- [16] S. Hosseini, R.J.D. Barroso, I.d. Miguel, Ó.G.d. Dios, N. Merayo, J.C. Aguado, P. Fernández, R.M. Lorenzo, E.J. Abril, Protection methods analysis in a hybrid C/C+L optical network, in: 2024 24th International Conference on Transparent Optical Networks, ICTON, 2024, pp. 1–4, http://dx.doi.org/10.1109/ICTON62926.2024.10648116.
- [17] M. Nakagawa, T. Seki, R. Hayashi, T. Kuwahara, Impact of wavelength-selective band switching on path protection in multi-band optical networks, in: ICC 2024 - IEEE International Conference on Communications, 2024, pp. 3047–3052, http://dx.doi.org/10.1109/ICC51166.2024.10622829.
- [18] M. Radovic, A. Sgambelluri, F. Cugini, N. Sambo, Power-aware high-capacity elastic optical networks, J. Opt. Commun. Netw. 16 (5) (2023) B16–B25.
- [19] J. Kundrát, E.L. Rouzic, J. Mårtensson, S. Melin, A. D'Amico, G. Grammel, G. Galimberti, V. Curri, MakeUppercaseGNPy: Lessons learned and future plans, in: 2022 European Conference on Optical Communication, ECOC, ISBN: 978-1-957171-15-9, 2022.
- [20] J. Simmons, Optical network design and planning, Optical Networks, vol. 2, Springer International Publishing, 2014.
- [21] V. Curri, M. Cantono, R. Gaudino, Elastic all-optical networks: A new paradigm enabled by the physical layer. How to optimize network performances? J. Lightwave Technol. 35 (6) (2017) 1211–1221.
- [22] E. Dijkstra, A note on two problems in connexion with graphs, Numer. Math. (1959).
- [23] A. Souza, N. Costa, J. Pedro, J. Pires, Comparison of fast quality of transmission estimation methods for MakeUppercaseC + MakeUppercaseL + MakeUppercaseS optical systems, J. Opt. Commun. Netw. 15 (11) (2023) F1–F12.

- [24] A. Mitra, D. Semrau, N. Gahlawat, A. Srivastava, P. Bayvel, A. Lord, Effect of channel launch power on fill margin in C+L band elastic optical networks, J. Lightwave Technol. 38 (5) (2020) 1032–1040.
- [25] International Telecommunication Union, Spectral Grids for WDM Applications: DWDM Frequency Grid, Recommendation ITU-T G.694.1, International Telecommunication Union, 2020, URL: http://handle.itu.int/11.1002/1000/ 14498. Edition 3.0.
- [26] J. Suurballe, R. Tarjan, A quick method for finding shortest pairs of disjoint paths, Netw. (1984).
- [28] J. O'Ramos, L. Cancela, J. Rebola, Impact of the reconfigurable optical add-drop multiplexer architecture on the design of multi-band C+L+S optical networks, Opt. Fiber Technol. 85 (2024) 103815.
- [29] J. Pedro, Designing transparent flexible-grid optical networks for maximum spectral efficiency, J. Opt. Commun. Netw. 9 (4) (2017) C35–C44.